The Use of Mass Spectrometry Imaging to Predict Treatment Response of Patient-Derived Xenograft Models of Triple-Negative Breast Cancer

Nadine E. Mascini,[†] Gert B. Eijkel,[†] Petra ter Brugge,[‡] Jos Jonkers,[‡] Jelle Wesseling,[‡] and Ron M. A. Heeren*[,†,§]

[†]Biomolecular Imaging Mass Spectrometry, FOM Institute AMOLF, Science Park 104, 1098 XG Amsterdam, The Netherlands

[‡]Divisions of Diagnostic Oncology & Molecular Pathology, Netherlands Cancer Institute − Antoni van Leeuwenhoek Hospital, Plesmanlaan 121, 1066 CX Amsterdam, The Netherlands

[§]The Maastricht Multimodal Molecular Imaging institute (M4I), Maastricht University, Universiteitssingel 50, 6229 ER Maastricht, The Netherlands

S *Supporting Information*

ABSTRACT: In recent years, mass spectrometry imaging (MSI) has been shown to be a promising technique in oncology. The effective application of MSI, however, is hampered by the complexity of the generated data. Bioinformatic approaches that reduce the complexity of these data are needed for the effective use in a (bio)medical setting. This holds especially for the analysis of tissue microarrays (TMA), which consist of hundreds of small tissue cores. Here we present an approach that combines MSI on tissue microarrays with principal component linear discriminant analysis (PCA-LDA) to predict treatment response. The feasibility of such an approach was evaluated on a set of patient-derived xenograft models of triple-negative breast cancer (TNBC). PCA-LDA was used to classify TNBC tumor tissues based on the proteomic information obtained with matrix-assisted laser desorption ionization (MALDI) MSI from the TMA surface. Classifiers based on two different tissue microarrays from the same tumor models showed overall classification accuracies between 59 and 77%, as determined by cross-validation. Reproducibility tests revealed that the two models were similar. A clear effect of intratumor heterogeneity of the classification scores was observed. These results demonstrate that the analysis of MALDI-MSI data by PCA-LDA is a valuable approach for the classification of treatment response and tumor heterogeneity in breast cancer.

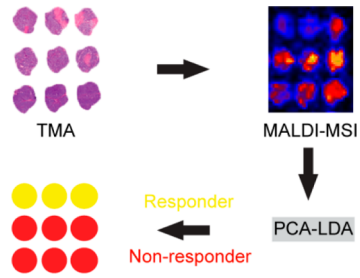

KEYWORDS: *mass spectrometry imaging, MALDI, tissue microarray, breast cancer, peptide profile*

INTRODUCTION

In cancer treatment, there is a great need to develop tools that can predict response to treatment. Mass spectrometry imaging (MSI) is a powerful analytical technique that provides complex molecular information to meet this objective. In particular, matrix-assisted laser desorption ionization (MALDI) MSI has shown its applicability to cancer research: it can probe intratumor heterogeneity,[1−3] and it can be used for tissue classification,[4−7] disease prognosis, and prediction of treatment response.[8−10] High-throughput analysis of clinical samples has been made possible by the establishment of protocols for the MALDI-MSI analysis of tissue microarrays (TMAs).[5,11] This has enabled the large-scale analysis of heterogeneous samples of limited quantity.

The analysis of TMAs with MSI easily generates thousands of spectra from hundreds of different tissue cores. In addition, each spectrum consists of hundreds of different molecular ions. Bioinformatic approaches that reduce this complexity are required to exploit the full potential of MSI. Up to now, a small number of studies have reported the use of PCA in combination with LDA or related statistical methods for the classification of MSI data.[7,12−14] PCA is used as dimensionality and noise reduction method, followed by LDA to build a classification model. Efficient separation of tissue type based on lipid profiles has been shown.[13−15] Also, disease-specific peptides and proteins could be identified in osteoarthritis and pancreatic cancer by this method.[7,12]

Here we report on the use of MALDI-MSI in combination with PCA-LDA to study the proteomic content of triple-negative breast cancer (TNBC) patient-derived xenograft (PDX) tumors. TNBCs account for ∼15% of breast cancers.[16] TNBC is characterized by the lack of expression of the estrogen receptor, progesterone receptor, and the human epidermal growth factor receptor type 2 (HER2). Therefore, it is considered difficult to treat because no targeted treatment is available yet for this subtype of breast cancer and resistance to conventional toxic chemotherapy frequently develops.[17,18]

Proteomic profiling of breast cancers has shown its usefulness for response prediction and the selection of more

effective treatment strategies.[8,9] In current practice, no reliable predictor of treatment response in TNBC before systemic treatment starts is available. The analysis of xenograft models by MALDI-MSI enabled us to study the proteomic content of these tumors under controlled conditions. For each tumor model multiple tissue cores were analyzed with MALDI-MSI and used to predict response to the chemotherapeutic drug cisplatin. Here we determine the predictive strength of MALDI-MSI data for treatment response using PCA-LDA. We also establish to which extent heterogeneity between the tissue cores from a particular tumor model compromises response prediction.

EXPERIMENTAL SECTION

Tissue Microarrays

The triple-negative PDX models had been specifically generated to study the mechanisms involved in chemotherapy response and acquired resistance. In a separate study, the models were treated with cisplatin, as clinical studies have shown a good response of TNBC to this cytotoxic drug.[19] The measured initial response of the models was categorized based on tumor size (Supporting Information Figure S-1): nine models responded well to the cisplatin treatment, resulting in a reduction of the tumor size ("good response"). Three models did not shrink or grow ("stable disease"), and seven showed reduced growth when compared with the control tumors ("progression"). Also, three models did not respond to the treatment ("no response").

Two TMAs (called hereafter TMA1 and TMA2) were constructed, both containing cores (triplicate 0.6 mm cores) from all 22 PDX breast cancer models. All tumor models were poorly differentiated (grade III) TNBCs as assessed by immunohistochemistry. The TMAs were constructed from treatment-naive samples. The TMA2 contained tissue cores from the same tissue blocks as TMA1, plus extra tissue cores from different tumors of the same PDX models. In this way, the reproducibility of the method and the tumor-to-tumor variation could be determined.

Tissue Preparation

Serial 5 μm sections were cut from the TMA blocks and mounted onto ITO-coated glass slides. The tissue cores were deparaffinized using xylene washes (100%, twice for 5 min) and rehydrated using graded ethanol washes (100% twice and 95%, 80%, and 70%, all 5 min), followed by water washes (twice, 3 min) to make the TMAs amenable to MALDI-MSI analysis. Antigen retrieval was performed by heating the slides in a 10 mM Tris buffer (pH 9.0) at 95 °C for 20 min. The slides were allowed to cool to room temperature, rinsed with water, and dried in a desiccator.

Local, on-tissue digestion was performed with trypsin, thereby preserving the spatial localization of the proteolytic peptides. A trypsin solution of 0.05 μg/μL was spotted in an automated manner (CHIP 1000, Shimadzu). A total of 5 nL was deposited per spot with a raster size of 200 × 200 μm. Trypsin spots measured ~100 μm in diameter. The sections were incubated overnight at 37 °C.

Finally, CHCA matrix solution was prepared at a concentration of 10 mg/mL in 50% ACN (v/v) and 0.1% TFA (v/v) in water and was sprayed onto the sections by a vibrational sprayer (ImagePrep, Bruker Daltonics).

MALDI-MSI Experiments

MALDI-MSI analyses were performed using a MALDI quadrupole time-of-flight SYNAPT HDMS mass spectrometer (Waters Corporation). The mass spectrometer was operated in TOF mode optimized for positively charged ions. Data were acquired in the range of m/z 200−3500 at a raster size of 150 μm. On average 16 spatially resolved spectra were recorded for each core.

Data Processing

Tissue core-specific spectra were extracted for data processing and subsequent statistical analysis. The spectra were subjected to peak detection using an in-house developed algorithm.[20] The ChemomeTricks toolbox for MATLAB was used for further preprocessing and analyses.[20] All spectra per core were averaged to create one representative spectrum per core. Averaged spectra per tissue core were used to reduce the influence of outliers in the data and improve the signal-to-noise-ratio. This approach improved the stability of the multivariate analysis results. A similar observation was reported by Gerbig et al.[13] Histological assessment of the tissue cores revealed that they were highly heterogeneous. Spectra were selected only from tissue regions with at least 80% tumor cells to reduce the variability caused by the presence of mostly stroma but also some necrotic regions. On average 13 spectra were selected per tissue core and used for subsequent analyses. This selection was compared with the full data set (on average 16 spectra per core) to determine the influence of the introduction of additional variability. An example of a heterogeneous tissue core can be found in Supporting Information Figure S-2.

Multivariate Statistical Approach

a. Data Sets. We performed multivariate statistical analyses on the data sets of both TMAs (TMA1 and TMA2). The aim was to identify a proteomic signature that could differentiate between the tumor models that did respond to the cisplatin treatment (responders) and the models that did not or hardly respond to the treatment (non-responders). For this purpose, tumor models that had experimentally shown to have a "good response" or "stable disease" were categorized as responders. Tumor models that had shown "no response" or "progression" were categorized as non-responders.

The average tissue core spectra were either assigned to the responder (n = 12) or non-responder (n = 10) class (Table 1).

Table 1. Samples Used for Construction of the Classifiers Based on TMA1 and TMA2

data set	response class	no. of tumor models	no. of tissue cores
TMA1	responder	12	70
	non-responder	10	51
TMA2	responder	12	113
	non-responder	10	67

On average six and eight tissue cores per tumor model were present in TMA1 and TMA2, respectively. Measurements of consecutive TMA sections were used to build the classifier. The data analysis workflow is summarized in Figure 1.

b. Principal Component Analysis. The spectra were normalized to their total ion count and the mass intensities were standardized to zero-mean and unit variance prior to PCA. PCA was performed on the average tissue core spectra with 3524 variables (mass intensities) each. PCA performs a linear

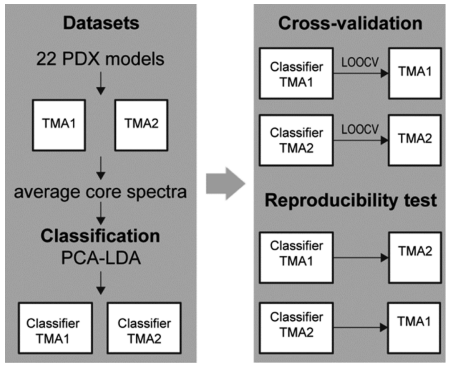

Figure 1. Summary of the data analysis workflow. The classifiers based on TMA1 and TMA2 are used to predict treatment response on the tumor, tissue core, and pixel (single spectrum) level.

transformation of the data in the direction of the largest variance. It defines new variables consisting of linear combinations of the original ones, so-called principal components (PCs). The first purpose of PCA was to reduce the dimensionality of the data. Second, PCA was employed to discard noise. It is important to note here that by using PCA it is assumed that the differences between the treatment response classes are one of the main sources of variation in the data and are thus described by the PCs. Otherwise these differences are lost in the PCA-based data reduction.

c. Linear Discriminant Analysis. Two individual classifiers were constructed based on TMA1 and TMA2, respectively. For this purpose, we used a two-step supervised classification method using a combination of PCA and LDA.[21] The PCs were used as input variables for the LDA. LDA calculates a linear combination of variables, in this case the PCs, that maximizes the ratio of the between-class variance and the within-class variance (Fisher's criterion). In other words, it finds the combination of PCs that leads to small discriminant score distances in LDA space within each class and large score distances between the classes. A tumor model is assigned to class *i* if the mean discriminant score of the tissue core spectra of this model is closest to the mean discriminant score of class *i*.

d. Double Cross-Validation. Classifiers built on highly dimensional data sets are prone to overfitting. It is, therefore, important to evaluate whether the classifier has been built with random fluctuations in the data or has predictive power. Classifiers are typically validated on independent samples. However, only 22 PDX models with tested initial treatment response were available. Instead, a leave-one-out cross-validation procedure was used to estimate the error rates of the classifiers. Leave-one-out cross-validation is an accepted validation method when the size of the data set is small.[22] Before anything else, the number of input PCs for the PCA-LDA needed to be estimated. This estimation was incorporated in the cross-validation by using a double leave-one-out cross-validation procedure as previously described to avoid the introduction of bias.[23]

The double leave-one-out cross-validation was performed as follows: all spectra from one tumor model were set apart as test spectra. Next, the optimal number of PCs was determined based on leave-one-out cross-validation using the spectra from the remaining 21 tumor models. The number of PCs to use was chosen based on optimal classification performance of the classifier, using the least number of PCs. The optimal number of PCs was 34 for the classifier based on TMA1 and 25 for the classifier based on TMA2. Then, the separate test tumor model was classified using the number of PCs as determined independently from the test tumor model. This procedure was repeated for all tumor models. Combined, the total number of misclassified tumor models gave an estimate of the error rate of the classifier.

e. Reproducibility Tests. The reproducibility of the method was evaluated by testing the classifiers using the alternate TMA. A classifier was trained on TMA1 and tested on TMA2 and vice versa. The same number of PCs was used as previously determined. The day-to-day variability was corrected using PCA-LDA as follows: each TMA data set was assigned a class. PCA-LDA was performed and the variance described by the resulting discriminant function was excluded from both data sets. The corrected data sets were used for the reproducibility tests.

RESULTS AND DISCUSSION

Predictions

The classifier based on TMA1 correctly predicted the treatment response for 17 out of 22 tumors, as determined by double cross-validation (Table 2). The classification model based on

Table 2. Classification Results for the Double Cross-Validations and the Reproducibility Tests Using the Alternate TMA as Training Set

data set		cross-validation		reproducibility test	
TMA1	tumor model	17/22	(77%)	15/22	(68%)
	tissue core	78/121	(64%)	76/121	(63%)
TMA2	tumor model	13/22	(59%)	18/22	(82%)
	tissue core	127/180	(71%)	125/180	(69%)

TMA2 had a classification accuracy of 13 out of 22 tumor models, of which 11 were also correctly classified based on the TMA1 classifier. The tissue core spectra classification scores for the cross-validation of TMA1 and TMA2 can be found in Figure 2. The correlation between the two models was quantified by calculating the correlation coefficients of the resulting loading plots and the average discriminant score per tumor model. The correlation coefficients were 0.73 and 0.82, respectively, indicating the similarity between the two models. Figure 3a shows the PCA-LDA loading plots of the TMA1 and TMA2 classifiers colored according to the extent of peptide peak contributions to the models. The images that depict the spatial distribution of exemplary peptide peaks with high loadings in both models are shown in Figure 3b.

Duplicate measurements of consecutive TMA sections resulted in very similar classification scores for each tumor model in the cross-validation (Supporting Information Figure S-3), giving an indication of the reproducibility of the method. Thus, the difference between the performances of the classifiers might be due to the different composition of the tissue microarrays of TMA1 and TMA2: only 40% of the tissue cores of TMA2 originated from the same tissue pieces as the tissue cores of TMA1. The remaining cores originated from different tumor pieces of the same PDX models.

Projection of the Predictions on the Pixel Level

The results can be visualized as a class image because spatial information is retained and remains associated with the spectra. The classification score for each pixel is plotted using a color code. Figure 4b shows the classification images for TMA1 and

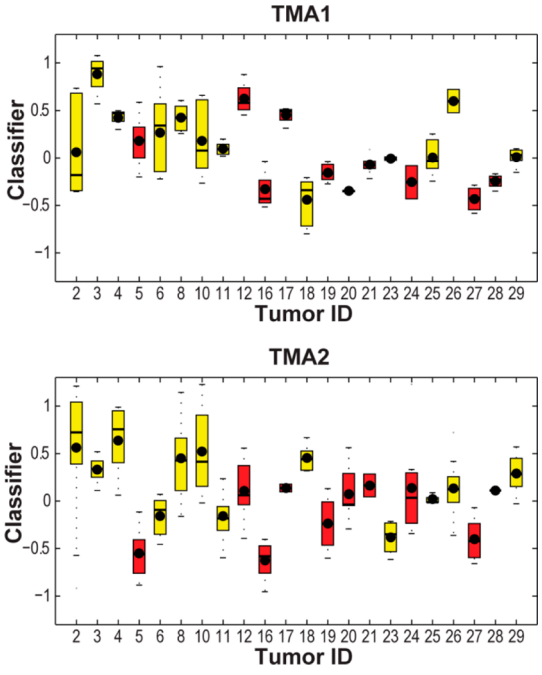

Figure 2. Box plots for the cross-validation of TMA1 and TMA2. The classification (discriminant function 1) scores are shown for the responder models (yellow) and the non-responder models (red). The classifier was constructed using the average core spectra from 21 tumors (training set), followed by classification of the spectra from the 22nd tumor (test set). Responder spectra are assigned positive values and non-responder spectra are assigned negative values in the classification models. The box plots represent the lower quartile, median (stripe), mean (dot), and upper quartile of the rescaled classification scores.

TMA2. The overall observed similarity of the scores for each tissue core gives an indication of the stability of the classifier. Tumor cores with ambiguous classification scores on the core level typically exhibit a mixture of yellow and red pixels, indicative for the heterogeneity of the tissue. Hematoxylin and eosin (H&E) stained adjacent sections from the entire TMAs can be found in Supporting Information Figure S-4.

Comparison of the Classifiers

a. On the Tissue Core Level. The reproducibility of the method was evaluated by testing the classifiers, which were both based on all 22 PDX models, using TMA1 as training set and TMA2 for validation as well as vice versa. It should be noted here that the two TMAs were analyzed independently from each other at more than half a year interval. In addition, the tissue core layout of TMA2 was completely randomized as compared with TMA1 to avoid bias introduced by the position of the tissue cores in the TMA. The reproducibility tests revealed 4 wrong predictions out of 22 for the TMA1 classifier and 7 out of 22 for the TMA2 classifier (Table 2). These results can be explained by the performance of the classifiers: 8 out of the 11 misclassifications in the reproducibility tests were also misclassified in the cross-validations. This means that these tumor models are not well described by the classifiers. It should be noted that the tumor models were assigned to two discrete classes only for the purpose of classification. It was expected that the intermediate response PDX models would be more difficult to classify than the "good" or "no response" PDX models. Unsurprisingly, the four most often misclassified tumor models were models with an intermediate experimental response, that is, "progression" or "stable disease". Supporting Information Figure S-5 shows the number of misclassifications per tumor model.

One would expect that variation between different tumors from the same PDX model might result in a poorer performance of the classifiers. However, a similar percentage of misclassifications was found for duplicate cores from the same tumor piece as for cores from different tumors of the same PDX model, yet the introduction of biological variation between the duplicate cores cannot be excluded because of the heterogeneity between the tumors within one PDX model system.

A duplicate tissue microarray for TMA1 was measured, at a year interval, to further test the reproducibility of the method. This new data set is predicted, using the classifier based on TMA1, with three misclassifications (8 of the 56 cores were misclassified). In line with our previous findings, those three tumor models were already determined to not fit well in the classification model based on TMA1. Proteomic differences between the duplicate tissue microarray and TMA1 cannot be excluded because the duplicate originated from another part of the TMA block.

b. On the Pixel Level. Figure 4c shows the classification maps for the reproducibility tests. The reproducibility test predictions are overall in agreement with the treatment responses. Similar predictions on the pixel level are observed for most tissue cores. However, also some heterogeneous predictions for single tissue cores are present, represented by mixed colors in the class images.

The extent of the observed heterogeneity in predictions was quantified as follows: for each PDX model the percentage of correctly classified pixels was determined, and this percentage was averaged over all data sets. Overall, 11 models show limited variation in classification score, defined as >70% or <30% correctly classified pixels (Supporting Information Figure S-6). The other models show a larger spread in classification scores. MALDI-MSI spectra are known to exhibit variability due to technical issues, for example, noise, the probing of mixtures of cells at the used spatial resolution and matrix preparation effects;[24] therefore improved reliability of classification can be obtained at the core or tumor level. A higher percentage of tissue cores with mixed prediction scores is present in TMA2 than in TMA1, reflecting the poorer separation achieved by the classifier based on TMA2. One would expect, from a histological perspective, that biomolecular heterogeneity gives rise to spectra with high variance. This heterogeneity might contribute to the observed distribution of classification scores. The classifiers will need to be tested on larger, homogeneous tissue sections to determine to which extent the spread in classification scores is caused by real tissue heterogeneity and not by technical variability.

In general, technical and biological variability between experiments limited the classification accuracies that were obtained, enhanced by the fact that the study was based on a small number of tumors. The small sample set was a reason for using LDA instead of a more complicated model with multiple free parameters. For example, genetic algorithms would not be very useful because they are prone to overfitting. An additional advantage of PCA-LDA is the possibility to evaluate the contribution of individual variables to the model. One would expect that different tumor classes have different peptide profiles that are revealed in the measurements. A follow-up study with clinical samples is required to externally validate

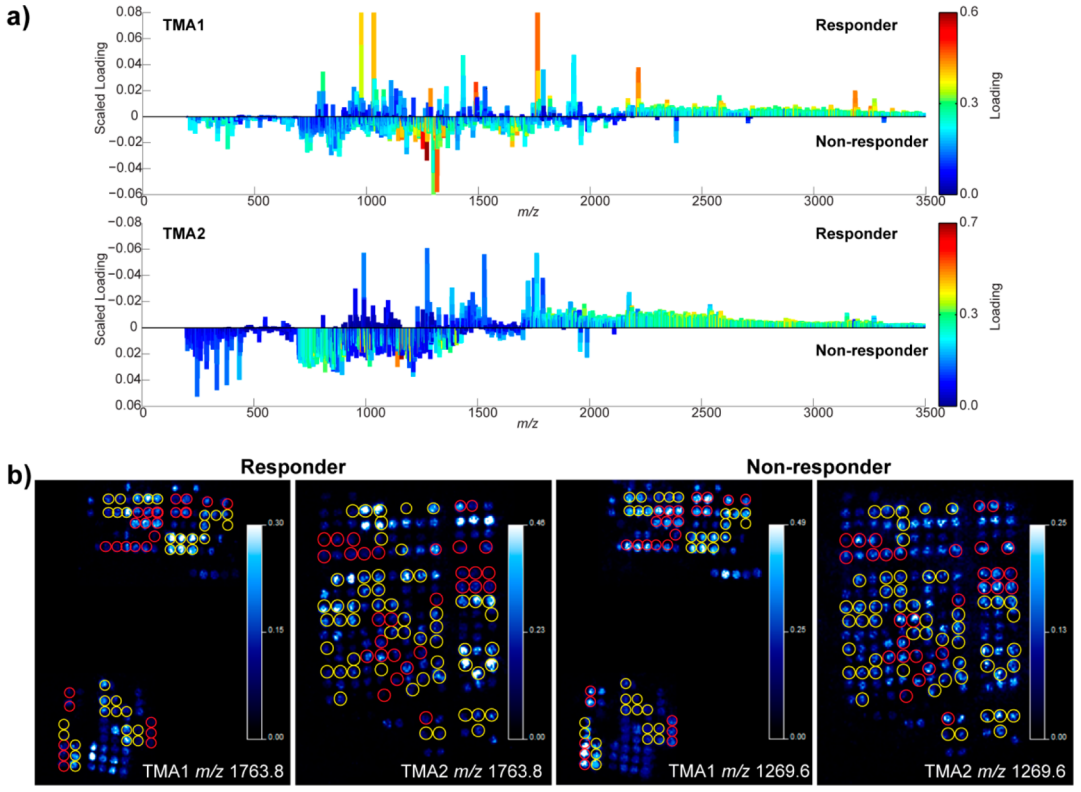

Figure 3. (a) PCA-LDA scaled loading plots of TMA1 and TMA2 colored as a function of variable (peptide peak) contribution in the projection. Scaling is applied by multiplying with the standard deviation of the original variables. (b) Selected ion images of variables with high loadings.

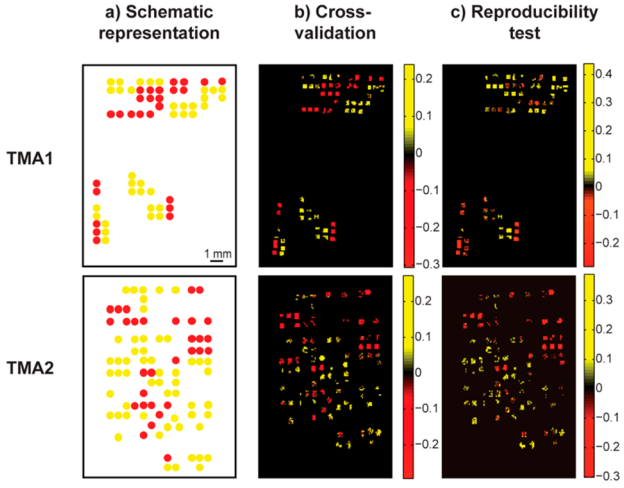

Figure 4. Classification results for TMA1 and TMA2 on the pixel level. The classification score for each spectrum is projected on its pixel location. (a) Schematic representation of the tissue microarrays with the responders (yellow) and non-responders (red). (b) Cross-validation classification scores. A clear difference between the responders and non-responders is observed. (c) Reproducibility test results for TMA1 and TMA2 on the pixel level. The TMA1 classifier was used to test the spectra from TMA2 and vice versa. Overall agreement between the schematic representation of the tissue microarrays and the reproducibility test results is observed. Also mixed color tissue cores are present. These cores show a heterogeneous classification: responder (yellow) pixels and non-responder (red) pixels are observed within one core.

these results. Moreover, the statistical approach might benefit from improved feature extraction. It is assumed in PCA-based feature extraction, as previously mentioned, that treatment response is one of the main sources of variation in the data. Variance, however, due to small differences between the treatment response classes might be poorly described by the PCs. These subtle changes, as for example differences in proteomic content in this study, can provide valuable information.

c. Taking into Account Tissue Heterogeneity. All results shown so far have been obtained with the spectra from regions with high tumor cell content. It is generally accepted, however, that the tumor microenvironment has an impact on treatment response.[25] New classifiers were built based on TMA1 and TMA2 using all spectra per core (SI Table S-1). Highly similar classification accuracies were obtained as compared with the accuracies previously reported. The new classifiers based on TMA1 and TMA2 correctly predicted the treatment response for 17 out of 22 and 14 out of 22 tumors, respectively (SI Table S-2). Interestingly, the reproducibility was increased. In particular, the classifier based on TMA2 showed a higher reproducibility (~20% higher). Histological analysis showed that the tumor cell content was on average the same in both treatment response classes (data not shown); therefore, an effect caused by an uneven distribution of tumor tissue can be excluded. Although it is difficult to find a biological interpretation of this result due to the "black box" nature of the experiment, it is clear that the included heterogeneity has a positive impact on the classification in this study.

CONCLUSIONS

In this work an approach is presented for the prediction of treatment response of PDX models of TNBC on the basis of MALDI-MSI data of TMAs. The results show its potential as a

tool to study and predict treatment response in a high-throughput way; hundreds of cores can be analyzed in a single measurement. In addition, the method described here permits the classification of treatment response with direct correlation to histologically defined regions of interest. We have described how multiple tumors from the same PDX model could be used to assess the reproducibility of the method, showing both technical and biological variability. Further development of multivariate statistical approaches will bring MSI closer to clinical application.

■ ASSOCIATED CONTENT

Supporting Information

Figure S-1: Examples of the measured treatment responses. Figure S-2: Optical images of H&E stained sections of the samples, showing the histological heterogeneity of the tissue cores. Figure S-3: Cross-validation results shown in Figure 2 for each measurement separately. Figure S-4. Optical images of H&E stained TMA sections. Figures S-5 and S-6: Additional information for the reproducibility test results: the total number of misclassifications per PDX model and the percentage of correctly classified pixels per PDX model. Tables S-1 and S-2: Samples used for the construction of the classifiers based on the complete data sets and the prediction results. This material is available free of charge via the Internet at http://pubs.acs.org.

■ AUTHOR INFORMATION

Corresponding Author

*Fax: +31-43-3884154. Tel: +31-43-3884199. E-mail: r.heeren@maastrichtuniversity.nl.

Notes

The authors declare no competing financial interest.

■ ACKNOWLEDGMENTS

This work is part of the research program of the Foundation for Fundamental Research on Matter (FOM), which is financially supported by The Netherlands Organization for Fundamental Research (NWO). N.E.M. and R.M.A.H. acknowledge financial support from the Dutch national program COMMIT.

■ REFERENCES

(1) Deininger, S. O.; Ebert, M. P.; Futterer, A.; Gerhard, M.; Rocken, C. MALDI imaging combined with hierarchical clustering as a new tool for the interpretation of complex human cancers. *J. Proteome Res.* **2008**, *7* (12), 5230−5236.

(2) Jones, E. A.; van Remoortere, A.; van Zeijl, R. J. M.; Hogendoorn, P. C. W.; Bovee, J. V. M. G.; Deelder, A. M.; McDonnell, L. A. Multiple Statistical Analysis Techniques Corroborate Intratumor Heterogeneity in Imaging Mass Spectrometry Datasets of Myxofibrosarcoma. *PLoS One* **2011**, *6* (9), e24913.

(3) Willems, S. M.; van Remoortere, A.; van Zeijl, R.; Deelder, A. M.; McDonnell, L. A.; Hogendoorn, P. C. W. Imaging mass spectrometry of myxoid sarcomas identifies proteins and lipids specific to tumour type and grade, and reveals biochemical intratumour heterogeneity. *J. Pathol.* **2010**, *222* (4), 400−409.

(4) Rauser, S.; Marquardt, C.; Balluff, B.; Deininger, S. O.; Albers, C.; Belau, E.; Hartmer, R.; Suckau, D.; Specht, K.; Ebert, M. P.; Schmitt, M.; Aubele, M.; Hofler, H.; Walch, A. Classification of HER2 receptor status in breast cancer tissues by MALDI imaging mass spectrometry. *J. Proteome Res.* **2010**, *9* (4), 1854−1863.

(5) Groseclose, M. R.; Massion, P. P.; Chaurand, P.; Caprioli, R. M. High-throughput proteomic analysis of formalin-fixed paraffin-embedded tissue microarrays using MALDI imaging mass spectrometry. *Proteomics* **2008**, *8* (18), 3715−3724.

(6) Meding, S.; Nitsche, U.; Balluff, B.; Elsner, M.; Rauser, S.; Schone, C.; Nipp, M.; Maak, M.; Feith, M.; Ebert, M. P.; Friess, H.; Langer, R.; Hofler, H.; Zitzelsberger, H.; Rosenberg, R.; Walch, A. Tumor classification of six common cancer types based on proteomic profiling by MALDI imaging. *J. Proteome Res.* **2012**, *11* (3), 1996−2003.

(7) Djidja, M. C.; Claude, E.; Snel, M. F.; Francese, S.; Scriven, P.; Carolan, V.; Clench, M. R. Novel molecular tumour classification using MALDI-mass spectrometry imaging of tissue micro-array. *Anal. Bioanal. Chem.* **2010**, *397* (2), 587−601.

(8) Reyzer, M. L.; Caldwell, R. L.; Dugger, T. C.; Forbes, J. T.; Ritter, C. A.; Guix, M.; Arteaga, C. L.; Caprioli, R. M. Early changes in protein expression detected by mass spectrometry predict tumor response to molecular therapeutics. *Cancer Res.* **2004**, *64* (24), 9093−9100.

(9) Bauer, J. A.; Chakravarthy, A. B.; Rosenbluth, J. M.; Mi, D.; Seeley, E. H.; De Matos Granja-Ingram, N.; Olivares, M. G.; Kelley, M. C.; Mayer, I. A.; Meszoely, I. M.; Means-Powell, J. A.; Johnson, K. N.; Tsai, C. J.; Ayers, G. D.; Sanders, M. E.; Schneider, R. J.; Formenti, S. C.; Caprioli, R. M.; Pietenpol, J. A. Identification of markers of taxane sensitivity using proteomic and genomic analyses of breast tumors from patients receiving neoadjuvant paclitaxel and radiation. *Clin. Cancer Res.* **2010**, *16* (2), 681−690.

(10) Aichler, M.; Elsner, M.; Ludyga, N.; Feuchtinger, A.; Zangen, V.; Maier, S. K.; Balluff, B.; Schone, C.; Hierber, L.; Braselmann, H.; Meding, S.; Rauser, S.; Zischka, H.; Aubele, M.; Schmitt, M.; Feith, M.; Hauck, S. M.; Ueffing, M.; Langer, R.; Kuester, B.; Zitzelsberger, H.; Hofler, H.; Walch, A. K. Clinical response to chemotherapy in oesophageal adenocarcinoma patients is linked to defects in mitochondria. *J. Pathol.* **2013**, *230* (4), 410−419.

(11) Casadonte, R.; Caprioli, R. M. Proteomic analysis of formalin-fixed paraffin-embedded tissue by MALDI imaging mass spectrometry. *Nat. Protoc.* **2011**, *6* (11), 1695−709.

(12) Cillero-Pastor, B.; Eijkel, G. B.; Kiss, A.; Blanco, F. J.; Heeren, R. M. Matrix-assisted laser desorption ionization-imaging mass spectrometry: a new methodology to study human osteoarthritic cartilage. *Arthritis Rheum.* **2013**, *65* (3), 710−720.

(13) Gerbig, S.; Golf, O.; Balog, J.; Denes, J.; Baranyai, Z.; Zarand, A.; Raso, E.; Timar, J.; Takats, Z. Analysis of colorectal adenocarcinoma tissue by desorption electrospray ionization mass spectrometric imaging. *Anal. Bioanal. Chem.* **2012**, *403* (8), 2315−2325.

(14) Veselkov, K. A.; Mirnezami, R.; Strittmatter, N.; Goldin, R. D.; Kinross, J.; Speller, A. V.; Abramov, T.; Jones, E. A.; Darzi, A.; Holmes, E.; Nicholson, J. K.; Takats, Z. Chemo-informatic strategy for imaging mass spectrometry-based hyperspectral profiling of lipid signatures in colorectal cancer. *Proc. Natl. Acad. Sci. U. S. A.* **2014**, *111* (3), 1216−1221.

(15) Cillero-Pastor, B.; Eijkel, G.; Kiss, A.; Blanco, F. J.; Heeren, R. M. Time-of-flight secondary ion mass spectrometry-based molecular distribution distinguishing healthy and osteoarthritic human cartilage. *Anal. Chem.* **2012**, *84* (21), 8909−8916.

(16) Bauer, K. R.; Brown, M.; Cress, R. D.; Parise, C. A.; Caggiano, V. Descriptive analysis of estrogen receptor (ER)-negative, progesterone receptor (PR)-negative, and HER2-negative invasive breast cancer, the so-called triple-negative phenotype: a population-based study from the California cancer Registry. *Cancer* **2007**, *109* (9), 1721−1728.

(17) Carey, L. A.; Dees, E. C.; Sawyer, L.; Gatti, L.; Moore, D. T.; Collichio, F.; Ollila, D. W.; Sartor, C. I.; Graham, M. L.; Perou, C. M. The triple negative paradox: primary tumor chemosensitivity of breast cancer subtypes. *Clin. Cancer Res.* **2007**, *13* (8), 2329−2334.

(18) Cleator, S.; Heller, W.; Coombes, R. C. Triple-negative breast cancer: therapeutic options. *Lancet Oncol.* **2007**, *8* (3), 235−244.

(19) Silver, D. P.; Richardson, A. L.; Eklund, A. C.; Wang, Z. C.; Szallasi, Z.; Li, Q.; Juul, N.; Leong, C. O.; Calogrias, D.; Buraimoh, A.; Fatima, A.; Gelman, R. S.; Ryan, P. D.; Tung, N. M.; De Nicolo, A.; Ganesan, S.; Miron, A.; Colin, C.; Sgroi, D. C.; Ellisen, L. W.; Winer, E. P.; Garber, J. E. Efficacy of neoadjuvant Cisplatin in triple-negative breast cancer. *J. Clin. Oncol.* **2010**, *28* (7), 1145−1153.

(20) Eijkel, G. B.; Kaletas, B. K.; van der Wiel, I. M.; Kros, J. M.; Luider, T. M.; Heeren, R. M. A. Correlating MALDI and SIMS imaging mass spectrometric datasets of biological tissue surfaces. *Surf. Interface Anal.* **2009**, *41* (8), 675−685.
(21) Hoogerbrugge, R.; Willig, S. J.; Kistemaker, P. G. Discriminant Analysis by Double Stage Principal Component Analysis. *Anal. Chem.* **1983**, *55* (11), 1710−1712.
(22) Simonetti, A. W.; Melssen, W. J.; van der Graaf, M.; Postma, G. J.; Heerschap, A.; Buydens, L. M. C. A chemometric approach for brain tumor classification using magnetic resonance imaging and spectroscopy. *Anal. Chem.* **2003**, *75* (20), 5352−5361.
(23) Hendriks, M. M. W. B.; Smit, S.; Akkermans, W. L. M. W.; Reijmers, T. H.; Eilers, P. H. C.; Hoefsloot, H. C. J.; Rubingh, C. M.; de Koster, C. G.; Aerts, J. M.; Smilde, A. K. How to distinguish healthy from diseased? Classification strategy for mass specitrometry-based clinical proteomics. *Proteomics* **2007**, *7* (20), 3672−3680.
(24) Alexandrov, T. MALDI imaging mass spectrometry: statistical data analysis and current computational challenges. *BMC Bioinf.* **2012**, 13.
(25) DeNardo, D. G.; Brennan, D. J.; Rexhepaj, E.; Ruffell, B.; Shiao, S. L.; Madden, S. F.; Gallagher, W. M.; Wadhwani, N.; Keil, S. D.; Junaid, S. A.; Rugo, H. S.; Hwang, E. S.; Jirstrom, K.; West, B. L.; Coussens, L. M. Leukocyte Complexity Predicts Breast Cancer Survival and Functionally Regulates Response to Chemotherapy. *Cancer Discovery* **2011**, *1* (1), 54−67.